AIAA 97-0555

Disturbance Evolution and Breakdown to Turbulence in a Hypersonic Boundary Layer: Ensemble-Averaged Structure

R. L. Kimmel and J. Poggie

Wright Laboratory
Wright-Patterson AFB, OH

35th Aerospace Sciences Meeting & Exhibit
January 6-10, 1997 / Reno, NV

DISTURBANCE EVOLUTION AND BREAKDOWN TO TURBULENCE IN A HYPERSONIC BOUNDARY LAYER: ENSEMBLE-AVERAGED STRUCTURE

Roger L. Kimmel*
and
Jonathan Poggie+
Wright Laboratory, Wright-Patterson AFB, Ohio 45433-7913

ABSTRACT

An experimental investigation of the spatial structure of second mode instability waves and their breakdown to turbulence was carried out in the boundary layer of a 7° half-angle, sharp-nosed cone at an edge Mach number of 6.8. Measurements were made at local Reynolds numbers of 2.3×10^6 to 9.1×10^6, spanning the range from unstable laminar to nearly turbulent flow. Simultaneous measurements with two hot film probes comprise the primary data set. Measurements were taken with circumferential, streamwise, and vertical probe separations. Broadband space-time cross correlations and wavenumber spectra were reconstructed from the ensemble averaged cross spectra of these signals. Results of circumferential cross correlations indicate that the second mode disturbances travel in wave packets of limited circumferential extent and circumferential wavenumber. Vertical correlation measurements indicate an evolution of the second mode disturbances from highly inclined structures with greatest intensity near the boundary layer edge, to more erect structures of shorter wavelength with high correlation near the wall.

NOMENCLATURE

f = frequency
k = azimuthal wavenumber, $2\pi r / \lambda_z$
k_n = maximum resolvable wavenumber
N = number of points per record
r = model radius
Re = Reynolds number base on conditions at boundary layer edge and running length along model
Re_u = unit Reynolds number based on freestream (upstream of model bow shock) conditions
S = wavenumber spectrum
U = velocity component parallel to model surface, at boundary layer edge
x = axial coordinate (Fig. 1), or time varying signal
X = Fourier component of signal x
y = circumferential coordinate (Fig. 1), or time varying signal
Y = Fourier component of signal y
z = vertical coordinate (Fig. 1)

δ = boundary layer thickness
ϕ = phase angle of eigenfunction
γ^2 = coherence
λ = wavelength
θ = phase angle of cross spectrum
τ = time delay in cross correlation
ξ = probe separation (Fig. 1)

INTRODUCTION

Boundary layer transition impacts hypersonic vehicle design through significant increases in heat transfer and skin friction that occur when the boundary layer transitions from laminar to turbulent flow. Transition predictions for hypersonic vehicle boundary layers are not yet reliable enough for satisfactory vehicle design. Uncertainty in transition location leads to diminished vehicle performance, primarily because of the additional weight of thermal protection needed to accommodate heating uncertainty. Improved understanding of the physics of hypersonic transition is required to validate computation and guide modeling.

It has been recognized for many years that stability theory forms a foundation for the prediction of transition and the interpretation of experimental results.[1,2] Stability theory predicts the growth and decay of periodic disturbances as a function of Reynolds number, over a range of frequencies and wavenumbers. It is likely that a broad spectrum of

*Aerospace Engineer, WL/FIMA, 2645 Fifth Street Suite 7. Senior Member AIAA.
+Aerospace Engineer, WL/FIMA, 2645 Fifth Street Suite 7. Member, AIAA.

wavenumbers and frequencies would be present in a flight environment to excite the boundary layer. Even measurements in "low turbulence" or "quiet" facilities which rely on the background spectrum of the wind tunnel to excite disturbances show a broad band of frequencies amplified over the range of unstable frequencies and nonlinear harmonics.[3, 4, 5] In addition to atmospheric turbulence and inhomogeneities over a range of scales, a thrusting hypersonic vehicle would experience vibration due to turbulent engine exhaust and a turbulent boundary layer over the aft of the vehicle. Such a vibration would not only cause a time-dependent displacement of the body, but would also cause a time-dependent distortion of the shock and create vorticity and acoustic waves.

Linear stability theory (LST), by definition, treats each frequency and wavenumber (both circumferential and streamwise) independently. It cannot account for nonlinear amplitudes and wave interactions. Eigenvalues and eigenfunctions for a spectrum of azimuthal and streamwise wavenumbers can be calculated, but not their interaction. Despite these limitations, LST has been successful at correlating some hypersonic transition results[5] and describing unstable frequencies and wavenumbers in hypersonic boundary layers.[6]

Parabolized Stability Equation (PSE) treatment offers the possibility of taking disturbance amplitude and nonlinear wave interaction into account. Herbert, et al.[7] and Malik et al.[8] have identified oblique wave interactions which give rise to longitudinal vorticity as a possible breakdown mechanism in the hypersonic boundary layer, based on PSE computations. Initial input to PSE requires initial disturbance amplitudes and their three-dimensional wave number spectrum. Full validation of the nonlinear interaction computations also requires spatially distributed measurements to resolve 3D oblique wave interactions.

Direct Navier Stokes Simulation (DNS), given sufficient computational resources, can compute farther into the breakdown regime than PSE. Pruett et al.[9] used DNS to calculate the breakdown of a boundary layer on an adiabatic wall cone with an edge Mach of 6.8. To alleviate the computational burden, PSE was used to calculate the linear and initial nonlinear disturbance growth. The PSE results were then fed in as initial conditions to the DNS. Pruett also showed oblique wave interactions as being important. Although 2D waves are most unstable for the dominant second mode instability,[1] a given wave at the above conditions initially evolves at lower Reynolds number as a first mode wave, for which oblique waves are most unstable. Computations[8, 9] indicate that oblique waves may play a significant role in the transition process due to their initial first mode growth history.

In each of these computational approaches, broadband inputs with continuous spectra are modeled with a finite number of wavenumbers. This requires judicious selection of the initial computational disturbance field. Numerical simulations of experiments where broadband input has been simulated by impulsive point disturbances have shown that the resulting wave packets may be represented in the small amplitude regime by a sum of linear modes.[10]

Previous validation experiments for hypersonic stability theory[11] have focused on obtaining spatial amplification rates from single-probe measurements. Nonlinear wave interactions have been observed experimentally,[12] but the full 2D and 3D wavenumber content cannot be extracted from these data. The goal of the current experiment was to obtain spatially and temporally resolved data using multiple probes to document the stability and breakdown of a hypersonic boundary layer. Multiple sensor measurements could be part of transition and stability flight experiments, and it is instructive to explore such measurements in a laboratory setting. Initial coherence and phase statistics from this experiment have been previously reported.[13] These coherence and phase data describe the spatial and temporal evolution of disturbances leading to transition. Part one of this paper further examines this detailed data set to extract ensemble averaged broadband and narrowband disturbance structure. These data provide a clearer picture of disturbance evolution. Since the disturbances are due to natural excitation, they are packet-like in nature, and their frequency and wavenumber content vary stochastically from ensemble to ensemble. To further resolve transition physics which are not resolved by ensemble averaging, Part two of this paper[14] examines instantaneous structure.

EXPERIMENT

Tests were carried out in Arnold Engineering Development Center (AEDC) Tunnel B, which is a closed circuit hypersonic wind tunnel with a 1.27 m diameter test section. Flow field surveys were made using a retractable overhead drive mechanism housed in an air lock immediately above the top of the Tunnel B

test section. An auxiliary on-board probe drive mechanism mounted on the model support sting was used to position a single probe in the model boundary layer at 0.895 m from the model apex. This mechanism traversed in the direction normal to the sting. More detailed descriptions of the tunnel may be found in other references.[13,15]

The basic model for the investigation was a 7° half-angle cone of 1.016 m length and 0.250 m base diameter, with interchangeable nose sections. In the present study, a sharp nose was used which had a spherical radius of 3.8×10^{-5} m. In order to minimize any interference with the flow in the base region of the model caused by the presence of the on-board probe drive mechanism, a frustum was added to the basic cone model. This 7° frustum extended the model length to 1.283 m and had a base diameter of 0.315 m. The frustum had a narrow slot which accommodated the movement of the strut which supported the probe mounted on the on-board drive mechanism. A sketch of the model and coordinate system are shown in Fig. 1.

The correlation measurements were carried out using custom-built hot film probes and constant-current anemometers. The anemometer signals were recorded on a Bell and Howell model VR3700B analog FM tape recorder. The film anemometer probe designs used in this experiment are described elsewhere.[13,16] Three channels of constant-current anemometer electronics were used. The anemometer amplifier contains the circuits required to electronically compensate the signal for a 6 db per octave roll-off which is characteristic of a hot-wire sensor. One can show[17] that the thermal-lag attenuation of the hot film probes is 3 db/octave, and the phase lag is 45°, over most of the frequency range of interest. Therefore no differential phase lag between probes was expected in this experiment. On the other hand, some quantitative distortions of the flow fluctuation spectrum were expected, because the compensating amplifiers used had a gain of 6 db/octave. However, these distortions were uniform for all probes and should have little effect on the measurement of narrow-band correlation coefficients. In broadband correlations the higher frequency components will be exaggerated due to their overcompensation. In most cases, the signal is dominated by a single second-mode frequency band, however, so there is little difference between the broadband and narrowband cross correlation.

Signal analysis was performed using an HP3562-A digital signal analyzer. The HP3562-A samples at 256 kHz, and the FM tape was played back at 1/8th speed for analysis, giving an effective sample rate of 2.048 MHz. Data were low-pass filtered below 1.024 MHz to prevent aliasing. The HP3562-A performed software fast Fourier transforms on the data, which provided the basis for the power and cross spectra. The cross spectrum of signals from two probes, designated 1 and 2, was obtained by multiplying the complex conjugate of the Fourier coefficient of signal 1 by the Fourier coefficient of signal 2, and averaging over N records. The cross-correlation of two signals was obtained from the inverse Fourier transform of the cross spectrum. The combined frequency-wavenumber spectrum is then obtained from a double Fourier transform of the cross correlation in space and time.

The above statistical quantities were averaged over $N = 120$ records of 2048 points each for streamwise and circumferential probe spacings, and $N = 60$ records of 2048 points each for vertical separations. Due to the stochastic nature of the signals and the finite record length, some statistical uncertainty, or rms error, is incurred which depends on the number of records and the coherence between the two signals. Generally, rms error decreases with increasing coherence and number of records.[18] The expected rms error for this experiment has been described previously.[13]

Test Conditions

The experiment was conducted at a freestream Mach number of 7.93. The stagnation temperature was 728 K, and the cone wall condition was adiabatic. Tests were carried out at freestream (upstream of the model bow shock) unit Reynolds numbers of $Re_u =$ 1.64×10^6, 3.28×10^6, 3.94×10^6, 4.92×10^6, 6.56×10^6 per meter by varying tunnel stagnation pressure. Measurements were carried out at a nominal x- location 0.895 m aft of the model tip, producing local x-Reynolds numbers of 2.3×10^6, 4.6×10^6, 5.5×10^6, 6.8×10^6, and 9.1×10^6 based on the local boundary layer edge unit Reynolds number and x- running length along the model surface.

One hot-film probe was mounted in the on-board drive at a fixed location x=0.895 m. A rake containing up to four additional hot film probes was mounted on the tunnel overhead drive. Measurements in the circumferential (or z) direction were carried out by positioning the probes

at the maximum energy location in the boundary layer, holding the rake fixed, and rolling the model to drive the on-board probe away from the rake (see sketch in Fig. 1). The maximum energy location is defined here as the y-location in the boundary layer at which the broadband rms signal from the hot film probe is a maximum. Measurements were taken at increments of 3.18 mm circumferential separation, up to 63.5 mm between the on-board probe and the rake probe nearest it. Streamwise correlations were obtained by holding the on-board probe fixed with a circumferential separation of 6.35 mm from the nearest rake probe, and moving the rake downstream in increments of 3.18 mm, up to 25.4 mm downstream of the on-board probe. The on-board probe was held fixed at the maximum energy location, and the downstream probe was relocated at the maximum energy point at each downstream station.

The boundary layer basic state was documented with surveys of mean Pitot pressure and total temperature. The boundary layer was laminar, but unstable, at the lowest Reynolds number, and near turbulent at the highest Reynolds number, based on boundary layer profile measurements and previous hot wire and heat transfer measurements.[13] During the boundary layer surveys, two additional hot film probes were mounted on the rake along with the Pitot and total temperature probes. These additional hot film probes were separated in the vertical (y) direction by 1.47 mm to obtain vertical correlations through the boundary layer.

RESULTS

Circumferential Probe Separation

Broadband space-time cross correlation coefficients for circumferential probe separation data at Reynolds numbers of $2.3\text{x}10^6$, $4.6\text{x}10^6$, and $5.5\text{x}10^6$ are shown in Fig. 2. The circumferential separation, ξ_z, is normalized by the boundary layer thickness, and the time delay τ is normalized by δ / U. Since the disturbances convect at near the edge velocity,[13] the τ axis approximates a streamwise separation normalized by δ. The disturbances are periodic in time (or streamwise direction), with a wavelength of approximately two boundary layer thicknesses, which is the second mode wavelength. This is expected, since spectra show the second mode to be dominant. The correlation is modulated in time and space, with a maximum at zero time delay, and drops off with increasing τ, approaching 0 at +/- 4 τ U / δ, reflecting the limited streamwise coherence of the signal and its packet structure.

Although Fig. 2 resembles wave packets observed by Gaster,[10,19] one must recall important differences between Fig. 2 and Gaster's results. Gaster presented contours of velocity fluctuations which were obtained by placing a hot wire at various x,z locations downstream of the disturbance source and ensemble averaging the signal. The Fig. 2 results were obtained by cross correlating two circumferentially separated probes. The second mode packets are presumed to be generated upstream, with some random distribution in time and space due to the stochastic nature of the freestream input disturbances. Fig. 2 thus presents a region in time and space over which second mode disturbances are coherent, and does not necessarily represent a disturbance amplitude level. The circumferential scale over which the signal is coherent is approximately 7.5δ or less for $\text{Re} \leq .4.6\text{x}10^6$.

Since the peak occurs at zero time delay for all circumferential separation, the second mode waves are, on average, two-dimensional, without any preferred obliquity. Since the cross correlation was reconstructed from the ensemble averaged cross spectrum, this is not unexpected. A random distribution of positively and negatively skewed waves would tend to cancel out during the ensemble averaging process. The instantaneous wave angle is addressed in the second part of this paper.

There is no evidence of a circumferential periodicity developing as Reynolds number increases, as might be expected from a subharmonic. Some variation in the optimum time delay with ξ_z is evident in the cross correlation obtained at Re = $4.6\text{x}10^6$. The predominant variation with Reynolds number is in the amplitude and circumferential scale of the correlation. Disturbances remain correlated out to a slightly larger ξ_z separation at Re = $2.3\text{x}10^6$ compared to $4.6\text{x}10^6$. Between Re = $4.6\text{x}10^6$ and $5.5\text{x}10^6$ there is a drastic rolloff in the circumferential correlation, although there is still a distinct streamwise periodicity at the second mode wavelength. Previous measurements[20] correlated Re = $4.6\text{x}10^6$ with transition on this configuration. The drop in correlation between these two Reynolds numbers indicates a rapid transition from the circumferentially organized second mode waves to structures with a much smaller circumferential scale. The transition front observed on shadowgraphs is

observed to fluctuate upstream and downstream to some degree. The observed cross correlation is probably the result of second mode wave packets alternated with turbulent, or quasi-turbulent flow which is circumferentially coherent only on a lesser scale.

A wavenumber spectrum derived from the circumferential correlations at 68 kHz (near the second mode peak at Re = 2.3×10^6) is shown in Fig. 3. The filtered cross correlation for f = 68 kHz at zero time delay was Fourier transformed with respect to circumferential separation to obtain the wavenumber spectrum. The data are normalized so that the area beneath the curve is one. The Nyquist, or maximum resolvable, wavenumber k_N, is equal to one-half the spatial sampling frequency in analogy with the temporal Nyquist frequency. Spatial anti-alias filtering is not possible with this configuration, but the roll-off in the wavenumber spectrum at higher wavenumber indicates that a significant portion of the higher wavenumber content was captured. The Nyquist wavenumber is 2.3 times the second mode streamwise wavenumber, and corresponds to an azimuthal wavenumber of 108. The lowest azimuthal wavenumber resolvable is 13.5. Note that if the circumferential extent of the wave packet is limited, there is no requirement that the azimuthal wavenumber be an integer. The circumferential wavenumber spectrum peaks at low wavenumber, but some energy content is distributed over higher wavenumbers.

Correlations were obtained in the freestream (upstream of the model bow shock) with the same probe configuration used for circumferential correlations in the boundary layer. The low signal level in the second mode frequency band in the freestream makes interpretation difficult. Donaldson and Coulter[21] showed that the shape of the freestream spectra was similar at different unit Reynolds numbers, but the maximum resolvable frequency increased with increasing unit Reynolds numbers. Their measurements at $Re_u = 9.8 \times 10^6$ /m show 0.07% mass flux and 0.013% total temperature fluctuations between 60 and 70 kHz, which is the second mode frequency band at $Re_u = 2.3 \times 10^6$ /m. $Re_u = 2.3 \times 10^6$ /m is a worst case. Since the freestream spectrum decreases with increasing frequency, the percentage freestream fluctuation in the second mode band drops as tunnel unit Reynolds number increases, due to the increasing second mode frequency. Freestream cross spectra were obtained at $Re_u = 3.9 \times 10^6$ /m in the current experiment. The coherence obtained from the cross spectrum in Fig. 4 show the signal to be uncorrelated above 50-75 kHz at minimum z separation in the freestream. The phase shows a large rms variation due to the low coherence level, but appears to be distributed about zero.

Vertical Probe Separation

The phase angle obtained by traversing two probes with a fixed vertical separation through the boundary layer was compared to linear stability calculations. The phase angle obtained from linear stability theory is the phase of the instability wave relative to the phase at some reference location. The phase angle obtained from the measured cross spectrum in this experiment is really the difference in disturbance phase between the two y locations. Therefore, a second order Runge-Kutta integration of the measured phase angle was carried out before it was compared to computation. Phase was referenced to zero at the first measurement point. A second consideration is that the phase depends on the quantity considered. The hot film anemometer voltage is a combination of its response to total temperature and mass flux fluctuations. Therefore, it is necessary to consider the computed phase of both total temperature and mass flux fluctuations.

The vertical probe separation was fixed at 1.47mm. Since the boundary layer thickness varied with tunnel unit Reynolds number, the probe separation in terms of δ varied from 0.189 δ to 0.314 δ. The effect of this vertical separation on the measured phase was assessed by simulating the measurement with the computed phase. The difference in the computed phase at the experimental locations was integrated using the same Runge-Kutta procedure used on the experimental data. The results in Fig. 5 show that the probe separation does indeed smear out the phase angle, but this smearing amounts to at most a 30 deg. error.

Experimental phase is compared to computed phase in Fig. 5. The experimental results agree with computed phase for total temperature fluctuations. The relative sensitivity of the hot film to total temperature and mass flux fluctuations depends on the hot film overheat ratio. At low overheats, the film is more sensitive to total temperature than mass flux fluctuations. The overheat ratio for the data shown in Fig. 5 was 13% (the film resistance was 13% higher than its resistance at recovery temperature). The Fig. 5 results are thus consistent with the relatively low overheats used in this experiment, and indicate that the probes were responding primarily to total temperature

fluctuations. These results show that even with the relatively large probe separation used in this experiment, this technique is useful for mapping disturbance eigenfunctions.

Broadband correlations derived from measurements made with probes separated vertically and traversed through the boundary layer are shown in Fig. 6. Since these measurements were made with a fixed probe separation, the reconstruction of the correlation contours requires some additional effort, similar to that described by Spina[22]. The survey point nearest the wall is taken as a reference. This correlation gives an optimum time delay for a fixed probe separation at this point in the boundary layer, $\tau_{max}(y_1)$. Given $\tau_{max}(y_1)$ and the distance between this point and the next survey point, $\Delta y = y_2 - y_1$, the correlation at y_2 is indexed in time by $(\Delta y / \xi_y)$ $\tau_{max}(y_1)$. Since the zero of the time delay axis is arbitrary in this scheme, the contours for convenience have been time-shifted to place the maximum positive correlation near the boundary layer edge at zero time delay.

The correlation should, in the context of linear stability theory, be unity across the boundary layer at the optimum time delay for each vertical point. Due to the presence of background disturbances and the extremely low signal level away from the edge of the boundary layer, the correlations at the lower Reynolds numbers drop off above and below the maximum energy location. The correlation contours thus reflect, to a certain extent, the signal-to-noise ratio. As the Reynolds number increases, the maximum correlation extends farther into the boundary layer. This indicates that the disturbance level in the interior of the boundary layer is increasing as the boundary layer progresses to turbulence.

The second mode waves at the lowest Reynolds number are periodic, with a streamwise wavelength of approximately two boundary layer thicknesses. The correlation persists several second mode wavelengths away from the zero reference. The waves tend to have a flattened or elongated structure. This agrees qualitatively with shadowgraphs of "rope" waves shown in Fig. 7 for the same configuration. Since the rope waves appear near boundary layer breakdown and have approximately the same wavelength as the second mode, they are most likely the second mode in a late, nonlinear stage of development. One must be careful not to make too literal a comparison between the shadowgraphs, which are images of the second derivative of density, and correlations of total temperature. Nevertheless, both show highly inclined wavefronts, i.e., large phase changes across the boundary layer. As the Reynolds number increases and the boundary layer begins to transition, the streamwise coherence length decreases and the disturbances begin to stand more erect (i.e., their phase shift in the y-direction decreases). At the highest Reynolds number, the angle between the correlation contours and the wall have increased further, reminiscent of typical "turbulent structures" seen in boundary layers.[22,23] Also, the dominant disturbances have shifted to a shorter wavelength, reflecting the spread of energy from the second mode to higher wavenumbers.

Bicoherence Analysis

Cross-bicoherence analysis between streamwise separated probes was carried out. Bicoherence on single channel measurements was also carried out. The bicoherence, defined as,

$$b^2(f_1,f_2) = \frac{\left|E\left[X(f_1)X(f_2)X^*(f_1+f_2)\right]\right|^2}{E\left[\left|X(f_1)X(f_2)\right|^2\right]E\left[\left|X(f_1+f_2)\right|^2\right]}$$

is a measure of nonlinear phase locking among frequency components in a single signal.[24] The cross bicoherence between signals x and y,

$$c^2(f_1,f_2) = \frac{\left|E\left[Y(f_1+f_2)X^*(f_1)X^*(f_2)\right]\right|^2}{E\left[\left|X(f_1)X(f_2)\right|^2\right]E\left[\left|Y(f_1+f_2)\right|^2\right]}$$

quantifies nonlinear phase locking among frequency components between two signals.[25] The bicoherence and cross-bicoherence vary from zero to one, where one indicates total quadratic coupling.

The cross-bicoherence was near zero at all Reynolds numbers in this experiment. Two factors probably account for this. First, at the lower Reynolds numbers, there was little nonlinear coupling. Second, the streamwise separated probes were also separated in the circumferential dimension by 6.35 mm to avoid interference. At higher Reynolds numbers, the circumferential correlations between probes dropped so rapidly that even at the minimum separation there was very little correlation.

The bicoherence measured at Re = 4.6×10^6, shown in Fig. 8, is essentially identical to the bicoherence measured using hot wire, rather than hot film, probes, and measured on the same model during a different test entry.[12] This emphasizes the

repeatibility of this nonlinear interaction, which has been observed in other boundary layers subjected to broadband input. Higher harmonics were observed in hypersonic transition in quiet facilities[3,4] and in subsonic flow with broadband acoustic input and roughness strips for acoustic receptivity.[5] The bicoherence measured at $Re = 5.5x10^6$, shown in Fig. 9, shows a broader range of nonlinear interactions. Nonlinear interaction of the subharmonic with itself and other frequencies is apparent in the bispectrum, although the subharmonic is not pronounced in the power spectrum.[11,13] The fundamental second mode also shows nonlinear interaction distributed across the spectrum. At both of these Reynolds numbers, the maximum bicoherence was approximately 0.4. This value is less than the maximum of one due to electronic noise and flow fluctuations.[12]

CONCLUSIONS AND FUTURE WORK

Space-time correlations in laminar and transitional boundary layers give a picture of the spatial structure of second mode waves and their breakdown. Most notably, the second mode waves are coherent over only a limited streamwise and circumferential extent. This behavior is no doubt due to the stochastic nature and limited spatial coherence of the disturbance sources. This gives rise to a circumferental wavenumber spectrum which is limited but broadband and continuous. There is no limitation that the azimuthal wavenumbers be integers. The turbulent "burst rings" observed by Fischer[26] on a cone in helium flow at Mach 18 would be an unlikely breakdown scenario for the current investigation.

The breakdown mechanism is dominated by the growth of nonlinear harmonics of the second mode and a filling in of the spectrum. The subharmonic is evident in the bicoherence, but is not prominant in the power spectrum. No circumferential periodicity was evident. Vertically separated probes were shown to be useful in extracting the disturbance phase, even with a fairly coarse vertical separation. These phase measurements demonstrated that the hot film probes with low overheat responded primarily to total temperature fluctuations.

The role of oblique wave interaction in the breakdown remains unresolved. Experiments with controlled disturbance generation would be useful to quantitatively measure nonlinear interactions. Advanced flow visualization techniques might help elucidate the breakdown mechanisms. The packet-like nature of the disturbances generated by broadband freestream inputs indicates that they might be successfully simulated experimentally and computationally by localized impulsive inputs to the boundary layer.

REFERENCES

[1] Mack, L. M., "Boundary-Layer Stability Theory," *Special Course on Stability and Transition of Laminar Flow*, edited by R. Michel, AGARD Report No. 709, 1984, pp. 3-1 to 3-81.

[2] Reshotko, E., "Stability Theory as a Guide to the Evaluation of Transition Data," *AIAA Journal*, Vol. 7, No. 6, 1969, pp. 1086-1091.

[3] Lachowicz, J. T., Chokani, N., and Wilkinson, S. P., "Boundary Layer Stability Measurements in a Hypersonic Quiet Tunnel," *AIAA Journal*, Vol. 34, No. 12, 1996, pp. 2496-2500.

[4] Doggett, G. P., Chokani, N., and Wilkinson, S. P., "Hypersonic Boundary-Layer Stability Experiments on a Flared-Cone Model at Angle of Attack in a Quiet Wind Tunnel," AIAA Paper 97-0557, Jan. 1997.

[5] Breuer, K. S., Dzenitis, E. G., Gunnarsson, J., and Ullmar, M., "Linear and nonliner evolution of boundary layer instabilities generated by acoustic-receptivity mechanisms," *Physics of Fluids*, vol. 8, no. 6, June 1996, pp. 1415-1423.

[6] Mack, L. M., "Boundary-Layer Stability Analysis for Sharp Cones at Zero Angle-of-Attack," Air Force Wright Aeronautical Laboratory Technical Report AFWAL-TR-86-3022, Aug. 1986.

[7] Herbert, Th., Stuckert, G. K., and Lin, N., "Method for Transition Prediction in High-Speed Boundary Layers," Air Force Wright Laboratory Technical Report WL-TR-93-3097, Sep. 1993.

[8] Chang, C.-L., and Malik, M. R., "Non-Parallel Stability of Compressible Boundary Layers," AIAA Paper 93-2912, July 1993.

[9] Pruett, C. D., and Chang, C.-L., "Spatial Direct Numerical Simulation of High-Speed Boundary-Layer Flows, Part II: Transition on a Cone in Mach 8 Flow," *Theoretical and Computational Fluid Dynamics*, vol. 7, 1995, pp 49-76.

[10] Gaster, M., "A theoretical model of a wave packet in the boundary layer on a flat plate," *Proceedings of the Royal Society of London*, vol. A. 347, pp. 271-289.

[11] Stetson, K. F., and Kimmel, R. L., "On Hypersonic Boundary-Layer Stability," AIAA Paper 92-0737, Jan. 1992.

[12] Kimmel, R. L., and Kendall, J. M., "Nonlinear Disturbances In a Hypersonic Laminar Boundary Layer," AIAA Paper 91-0320, Jan. 1991.

[13] Kimmel, R. L., Demetriades, A. , and Donaldson, J., "Space-Time Correlation Measurements in a

Hypersonic Transitonal Boundary Layer," *AIAA Journal*, Vol. 34, No. 12, 1996, pp. 2484-2489.

[14] Poggie, J., and Kimmel, R. L., "Disturbance Evolution and Breakdown to Turbulence in a Hypersonic Boundary Layer: Instantaneous Structure," AIAA Paper 97-0556, Jan. 1997.

[15] Boudreau, A. H., "Performance and Operational Characteristics of AEDC/VKF Tunnels A, B, and C," Arnold Engineering Development Center Technical Report AEDC-TR-80-48 (AD A102614), Jul. 1981.

[16] Demetriades, A., and Anders, S. G., "Characteristics of Hot Film Anemometers for Use in Hypersonic Flows," *AIAA Journal*, Vol. 28, No. 11, 1990, pp. 2003-2005.

[17] Demetriades, A., "Frequency Response of Constant-Current Film Anemometers," *International Journal of Heat and Mass Transfer*, Vol. 36, No. 1, 1993, pp. 231-232.

[18] Bendat, J.S., and Piersol, A. G., *Random Data Analysis and Measurement Procedures,* 2nd ed., John Wiley and Sons, New York, 1986, pp. 294-302.

[19] Gaster, M., and Grant, I., "An experimental investigation of the formation and development of a wave packet in a laminar boundary layer," *Proceedings of the Royal Society of London*, vol. A. 347, pp. 253-269.

[20] Stetson, K. F., Thompson, E. R., Donaldson, J.D., and Siler, L. G., "Laminar Boundary Layer Stability Experiments on a Cone at Mach 8, Part 1: Sharp Cone," AIAA paper 83-1761, Jul. 1983.

[21] Donaldson, J., and Coulter, S., "A Review of Free-Stream Flow Fluctuation and Steady-State Flow Quality Measurements in the AEDC/VKF Supersonic Tunnel A and Hypersonic Tunnel B," AIAA paper 95-6137, April 1995.

[22] Spina, E. F., Donovan, J. F., and Smits, A. J., "On the structure of high-Reynolds-number supersonic turbulent boundary layers," *Journal of Fluid Mechanics*, vol. 222, 1991, pp 293-327.

[23] Owen, F. K., and Horstman, C. C., "Hypersonic Transitional Boundary Layers," *AIAA Journal*, Vol. 10, No. 6, 1972, pp. 769-775.

[24] Nikias, C. L. and Raghuveer, M. R., "Bispectrum Estimation: A Digital Signal Processing Framework," *Proceedings of the IEEE*, Vol. 75, no. 7, Jul. 1987, pp. 869-891.

[25] Hajj, M., Miksad, R., and Powers, E., "Experimental Investigation of the Fundamental-Subharmonic Coupling: Effect of the Initial Phase Difference," AIAA paper 91-0624, Jan. 1991.

[26] Fischer, M. C., "Turbulent Bursts and Rings on a Cone in Helium at $M_e = 7.6$," *AIAA Journal*, vol. 10, no. 10, October 1972, pp. 1387-1389.

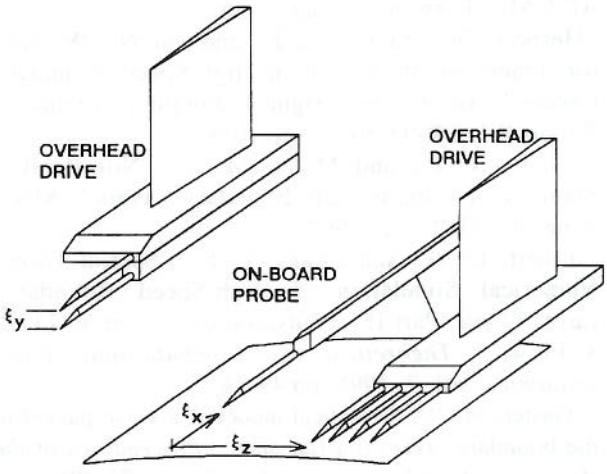

Figure 1. Coordinate System

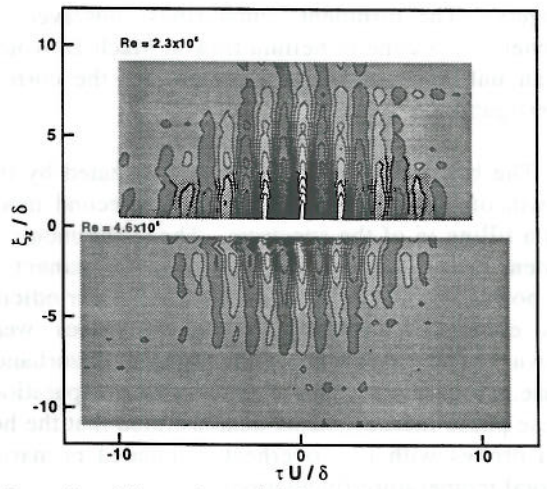

Figure 2a. Circumferential Correlations at Re = 2.3×10^6 and 4.6×10^6.

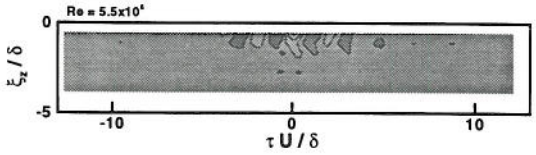

Figure 2b. Circumferential correlations, cont'd.

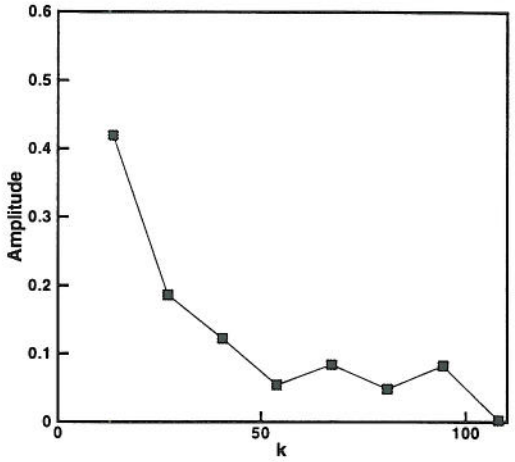

Figure 3. Circumferential wavenumber spectrum for f = 68 kHz at Re = 2.3×10^6.

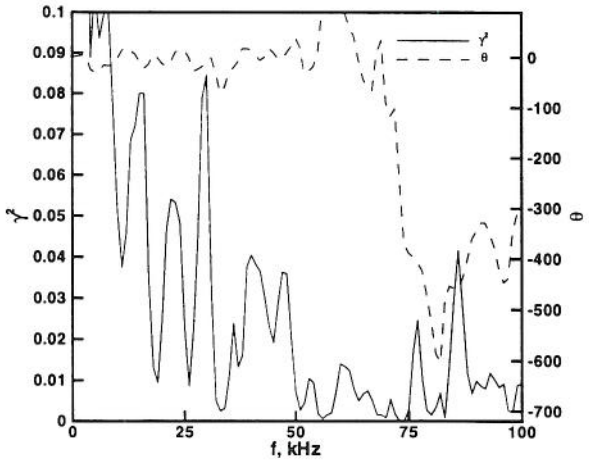

Figure 4. Freestrem coherence and phase.

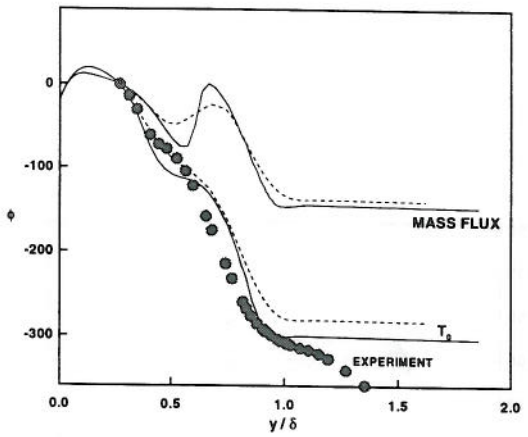

Figure 5. Phase angle through boundary layer. Dashed lines indicate effect of finite probe spacing on computed phase angles

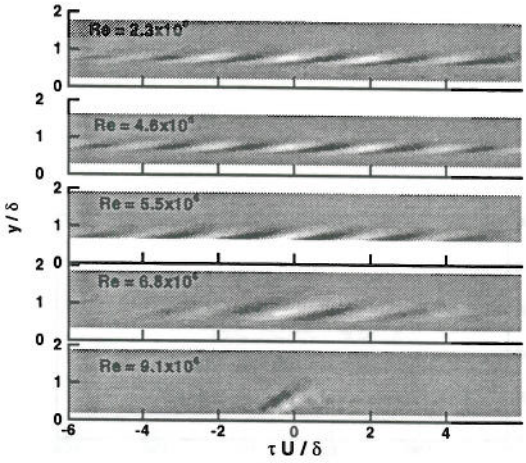

Figure 6. Vertical Correlations

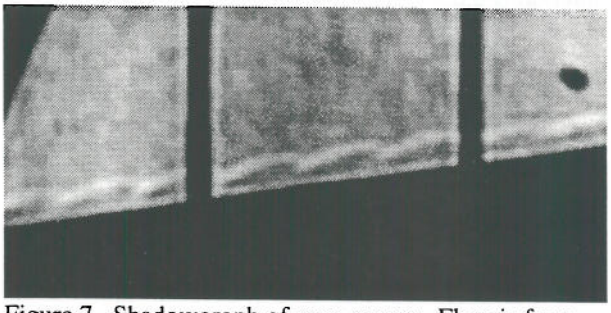

Figure 7. Shadowgraph of rope waves. Flow is from left to right.

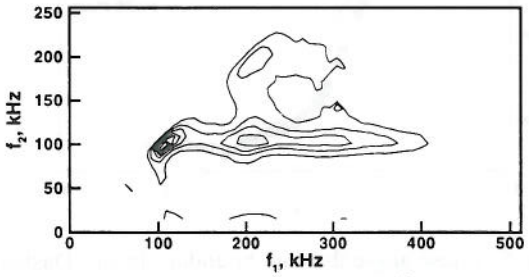

Figure 8. Bicoherence at Re = 4.6×10^6. Contour interval is 0.05.

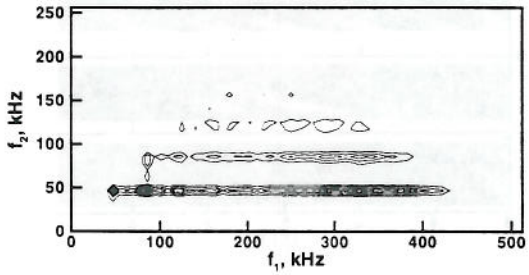

Figure 9. Bicoherence at Re = 5.5×10^6. Contour interval is 0.05.